RILEM-*fib*-AFGC Int. Symposium on Ultra-High Performance Fibre-Reinforced Concrete,
UHPFRC 2013 – October 1-3, 2013, Marseille, France

ANALYSIS OF A UHPFRC FOOTBRIDGE WITH A DECK SLAB UNDER BENDING BY A NOVEL FRACTURE-MICROMECHANICS FEM MODEL

Thomas Guénet (1-2), Luca Sorelli (1), Dominique Corvez (3), Josée Bastien (1), François Toutlemonde (2), Emmanuel Ferrier (4) and Laurent Michel (4)

(1) CRIB, Université Laval, Québec, Canada

(2) UPE-IFSTTAR, Marne-la-Vallée, France

(3) Lafarge, Paris, France

(4) Université Claude Bernard Lyon 1, Villeurbanne, France

Abstract

Ultra High Performance Fibre Reinforced Concrete (UHPFRC) structures are emerging in several engineering applications as their outstanding tensile strength and ductility allow engineers to develop new structural concepts and overcome construction limits. This paper focuses on the structural analysis of a new UHPFRC deck footbridge originally designed for Blandan Park in Lyon, France using a new fracture micromechanics Finite Element model. The latter was recently developed to describe the fibre pullout and the matrix cracking within the framework of fracture mechanics. The orientation of fibres was taken into account by statistically averaging a micro-mechanical model which describes debonding and pulling out of fibres from a cement matrix. We first calibrated the model parameters on the stress-strain relationship derived from 3-point bending tests of UHPFRC with 1.25 % stainless steel fibres. Different casting procedures were simulated by changing dispersion on fibre orientation.

Résumé

Les structures en BFUP font leur apparition dans de nombreuses applications d'ingénierie grâce à l'excellente résistance en traction de ces matériaux, qui permet aux ingénieurs de développer de nouveaux concepts de structure et de dépasser les limites de construction actuelles. Ce document met l'accent sur l'analyse structurelle d'une nouvelle passerelle cantilever en BFUP conçue pour le parc Blandan à Lyon. Pour profiter du comportement en traction des BFUP, un nouveau modèle micromécanique est développé dans le cadre de la mécanique de la rupture, il décrit la dissipation d'énergie par les fibres et le comportement non linéaire de la matrice. L'orientation des fibres est prise en compte par une modélisation micromécanique de l'arrachement des fibres et permet une estimation de la ductilité de la structure. Les paramètres du modèle sont calibrés à partir de la loi de comportement en contrainte et déformation extraite à partir d'essais de flexion trois points de BFUP avec 1,25 % de fibres d'acier inoxydable. Différentes procédures de mise en œuvre sont étudiées en changeant la dispersion sur l'orientation des fibres.

1. INTRODUCTION

Fibres have an important effect on the mechanical properties of UHPFRC, especially for achieving the hardening behaviour after first cracking. Notably, experiments showed that the structural ductility of UHPFRC beams strongly depends on the fibre orientation. As a consequence, the structural behaviour of UHPFRC may depend on the casting methods [1-2]. Moreover, the fibre orientation may cause unfavourable size effect when the structural behaviour of UHPFRC laboratory tests is compared to that of full-scale structures. As a consequence, the design of UHPFRC structures needs to consider fibre orientation effects, especially for thin structures where fibre orientation is affected by shear flow and wall effect.

Most of models available in open literature, like Willam-Warnke [3], Lubliner [4-5], Feenstra and de Borst [6], are phenomenological and thus not suitable to model fibre orientation. Instead, the existing micromechanical models which consider fibre orientation, assume a uniform fibre orientation resulting in an unrealistic isotropic behaviour [7-8].

In this paper, we employed a new fracture micro-mechanics model which has been lately developed to describe energy contribution of fibre in the crack growth as detailed in Sorelli *et al.* [9-11]. In this work, we briefly describe the key features of the model. The fibre orientation is considered by a Gaussian-like probability density function rather than a uniform one. The model is then calibrated on experimental results. Then, the FEM implementation of the micromechanics model is applied to study the bending tests of a footbridge made of a cantilever deck reinforced with 1.25 % stainless fibres. Finally, the effect of the casting procedure was simulated by varying the dispersion on fibre orientation.

2. EXPERIMENTAL DATA

The experimental test aimed at defining the bending behaviour of a cantilever deck cast with a Ductal® stainless steel fibre reinforced UHPC. Fibres are 14 mm long with a diameter of 0.185 mm. The fibre volume fraction is 1.25 % and the elastic modulus is 50 GPa. The UHPFRC used in this contribution has a compressive strength of 150 MPa with thermal treatment and 130 MPa without and it respects AFGC recommendation on ductility [12].

The structure is a cantilever deck footbridge originally designed for Blandan Park in Lyon, France [12]. A half-scaled version was tested under bending. The tested structure is composed of a 20 mm thick slab, 3.775 m long and 1.15 m wide, reinforced with longitudinal and transversal elements as shown in Fig. 1. Three reinforcement bars with 20 mm of radius, are displayed in the upper part of the longitudinal beam (in the central rib).

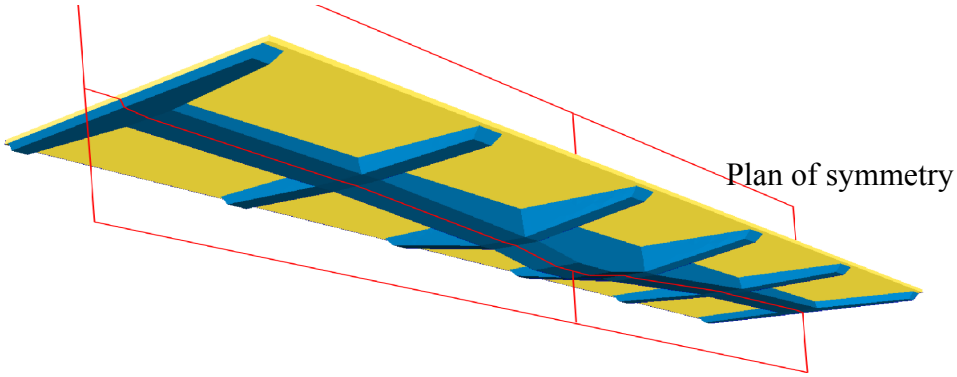

Figure 1: 3D view of the cantilever deck footbridge

Figure 2 shows how the eight LVDT and six strain gauges (120 Ω and 30 mm long) were dispatched on the structure. The footbridge was tested under bending. The structure was simply supported in the mid-span section. One end was vertically fixed with two steel frames, while a concentrated force was applied on the other end. The displacement was controlled by a hydraulic jack with a displacement rate of 5 mm/min. The deck broke in compression after a maximal deflection of 178 mm. The central rib slightly cracked in compression while the slab developed multiple macro cracks. Experimental results of LVDT 1 and 2, and strain gauges 1 to 6 are presented in section 4.

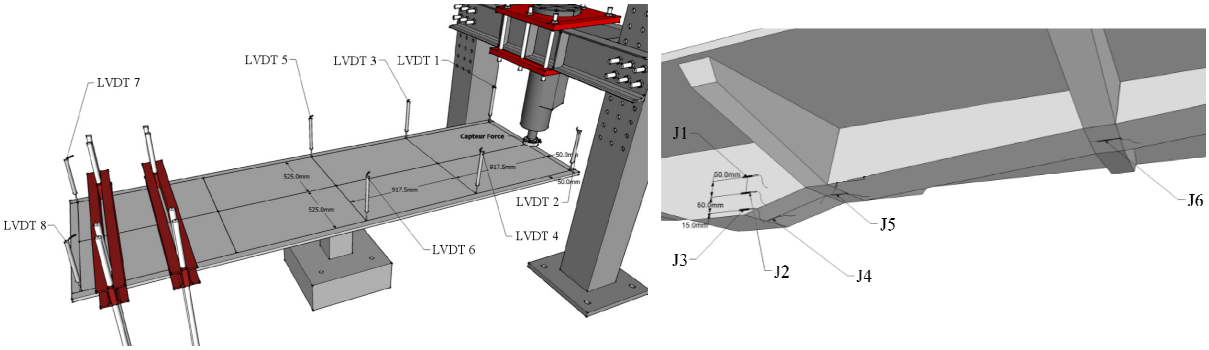

Figure 2: LVDT and strain gauges locations

3. FEM MODELING

3.1 New damage micromechanics model

Considering a Representative Element Volume (REV) of the material, we identify two systems of loads: the external loads and the fibre bridging forces which have opposite directions. According to Linear Elastic Fracture Mechanics (LEFM), the resulting stress intensity factor is the difference between the stress intensity factors of each load. Considering the Irwin relationship ($G = K^2 / E$), the energy release rate can be formulated as proposed by Bažant [13]:

$$f = \mathrm{G_A} + \mathrm{G_B} - 2\sqrt{\mathrm{G_A}\,\mathrm{G_B}} - \mathrm{G_c}, \tag{1}$$

where $\mathrm{G_A}$ is the energy release rate of the external loads: it is defined as the derivative of the free energy Ψ, by damage parameter $e \equiv N_c\, a^3$, defined by Budiansky in [14], assuming a penny-cracked shape of radius a and the Mori-Tanaka homogenization scheme [15] which takes into account microcracks interaction. The resulting stiffness tensor is transverse-isotropic as follows the micromechanics model proposed by Dormieux et al. [16]. We limited this preliminary work to study the mode I fracture type by considering only one family of parallel cracks.

$$\mathrm{G_B} = N_c \frac{\partial a}{\partial e} \frac{\partial W(e)}{\partial e} \tag{2}$$

is the energy release rate which takes into account the contribution of fibres as defined in [7], where

$$W(a) = 2p \int_0^a \int_0^w s_c(w)\, r \, \mathrm{d}w \mathrm{d}r \text{, with } w \le L_f / 2 \tag{3}$$

is the energy dissipated by fibres when forming a penny-shaped crack of radius a. σ_c is the composite fibre stress proposed by Lin et al. [8], as described in Sec. 3.3; it is first integrated according to crack opening before being integrated over the crack. G_f is the fracture energy of the matrix, N_c number of cracks per mm^3 and G_c the equivalent fracture energy of the REV written as a function of the damage parameter. The loading function Eq. (1) fulfils the loading-unloading condition, also called Kuhn-Tucker form:

$$f(e) < 0; \quad f(e)\, de = 0; \quad de \geq 0. \tag{4}$$

By solving system of Eq. (4) for a given strain history along with the consistency condition $df = 0$, the stress-strain material law of the material beyond the elastic part is derived.

3.2 Probability Distribution of fibres orientation

The casting procedure has an important effect on the fibre orientation. The fibre orientation distribution is taken as a π-periodic Gaussian like probability distribution function $p(\theta,\varphi)$ as follows, plotted in Fig. 3:

$$p(\theta,\varphi) = k_g/(2\pi \sinh k_g) \cosh[k_g (\cos\varphi \cos\varphi_0 - \sin\varphi \sin\theta \sin\varphi_0)] \tag{5}$$

where (θ,φ) are the spherical coordinates, and the parameters k_g and φ_0 are respectively, the degree of uniformity and the angle between the symmetric axis of the distribution and the normal direction of the crack plane, which is axis z on Fig. 3. The assumed probability distribution function is normalized so that $\iint p(\theta,\varphi) \sin\varphi \, d\varphi \, d\theta = 1$.

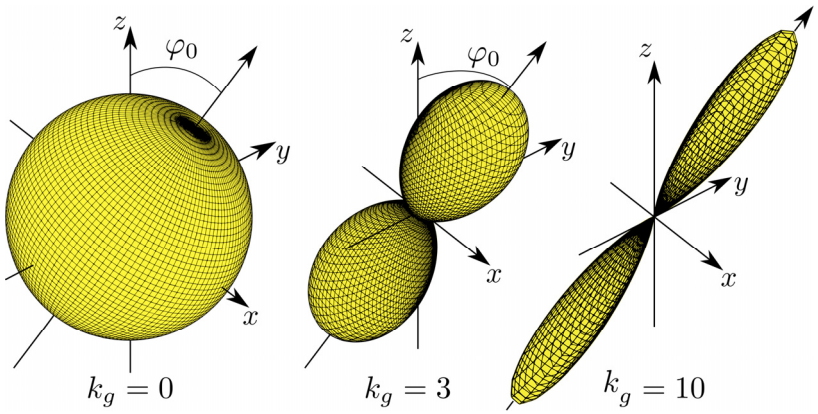

Figure 3: Graphical representation of the probability distribution function of the fibre orientation for three different values of k_g, where the x-y plan is the crack plan

The probability that fibres are aligned in a chosen direction corresponds to the distance between the origin of the coordinate system and the intersecting point between that direction and the surface of the distribution. Table 1 gives examples of values correspondence between the standard orientation factor α also known as the percentage of fibres intercepting the crack plan and the disparity parameter of fibres k_g (for $\varphi_0 = 0$).

Table 1: Correspondence between parameter k_g and orientation coefficient α

k_g	0	2.206	3	10
α	0.500	0.637	0.698	0.900

3.3 Fibre pull-out mechanism

The composite fibre stress σ_c is derived from the integration over the REV of the fibre pull-out force multiplied by the probability that the fibre intercepts the crack plane as proposed by Lin *et al.* [8].

$$s_{\mathrm{c}} = 4\frac{v_f}{p d_f^2}\int_0^{2p}\int_0^{2p}\int_0^{p/2\cos j} \mathrm{F}(\mathrm{w})h(j\ )p(z)\,p(q,j\ )\,\sin j\ \ \mathrm{d}z\,\mathrm{d}j\ \ \mathrm{d}q \tag{6}$$

where z is the distance of centroid of fibre from crack plan and $p(z)$ its probability distribution. $p(z) = 2/L_f$ is chosen uniformly distributed in the REV. η accounts for the mechanical effect of the fibre inclination on the pull-out curve. As for steel fibres, Naaman *et al.* showed that η is mostly 100 % for the fibre inclination from 0 to of 70 % [17]. For the UHPFRC studied, which is reinforced with steel fibres, we considered the mechanical effect as secondary with respect to the probability of intercepting a crack. The relationship between the debonding force F_d and the post-debonding force F_p with respect to the crack opening displacement was originally proposed by Leung *et al.* [18]. For $0 < w \leq w_0$:

$$\mathrm{F_d}(w) = \frac{1}{2} d_f p \sqrt{(1+c)t_0 E_f d_f w}\,, \tag{7}$$

and for $w_0 < w \leq L_f/2$:

$$F_p(w) = p\,d_f\,t_0\frac{1+c}{L - w + w_0}\,, \tag{8}$$

with

$$c = \frac{E_f v_f}{E_m(1-v_f)} \quad \text{and} \quad w_0 = \frac{4(1+c)t_0 L^2}{E_f d_f}\,, \tag{9}$$

where d_f: fibre diameter; E_f: fibre module of elasticity; E_m: matrix module of elasticity; v_f: volume of fibres; L: embedded length of fibre; τ_0: bond strength of fibre-matrix interface and w_0 is the crack opening displacement at which the fibre is fully debonded. Note that the possibility of a debonding effect due to the Poisson's ratio is not considered in the model, while the group effect of fibres is indirectly taken into account in the calibration of the fibre bond strength.

3.4 Material Model Calibration

The model has been calibrated on the average strain-stress relationship obtained from reverse analysis on 70 x 70 x 280 mm notched specimens under three-point bending tests with fibre volume of 1 % and 1.5 % [12]. Table 2 is a list of calibrated values and Fig. 4 shows the resulting calibrated model.

Table 2: Fibre and matrix model parameters.

E_m	v	G_f	τ_0	L_0	
45 GPa	0.18	0.0637 J/m^2	13 MPa	150 mm	
v_f	L_f	d_f	E_f	k_g	e_0
1.25 %	14 mm	0.185 mm	210 GPa	0	0.0003

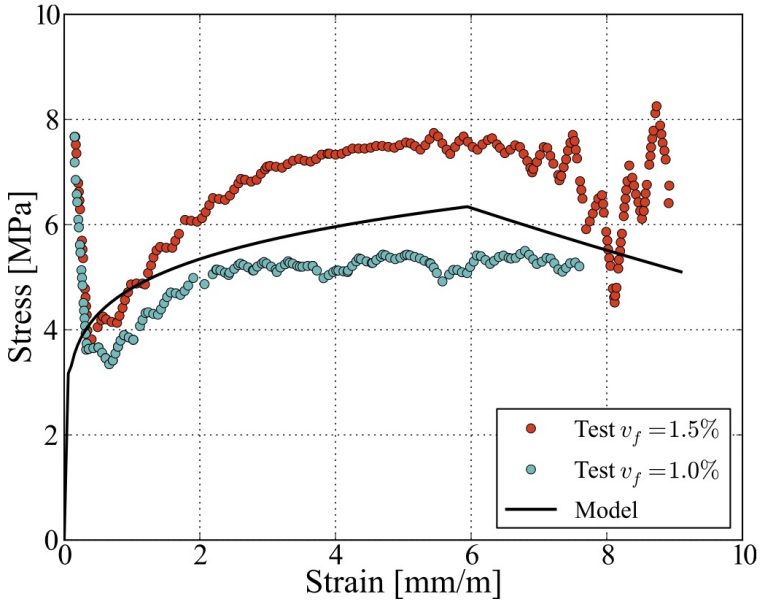

Figure 4: Model calibration on strain-stress relationship

Although the model would have been able to capture the load drop due to first cracking by setting a lower initial crack density and increasing the fracture energy of the matrix, we preferred to carry out those preliminary tests without the stress drop for avoiding numerical issues of convergence. Neglecting the stress drop can cause an underestimation of the structural behaviour. This assumption can be acceptable for the cases when the peak load of the structure is reached with a zone of inelastic points which have developed an advanced inelastic state (e.g., plastic hinge), while the rest of the structure is elastic; such assumption is confirmed afterwards by results shown in next section and Fig. 6. The specific fracture energy of the matrix (G_f) is reduced to have a smooth strain-stress law without the stress drop. The bond strength of fibre-matrix interface (τ_0) is used to set the maximal tensile stress according to literature values, between 10 and 18 MPa [19]. The initial damage parameter (e_0) is calibrated to set the strain corresponding to maximal stress. Then the characteristic length (L_0) is calibrated to capture the softening curve only and the disparity of fibres (k_g) is chosen according to [12] which specified that fibres have an isotropic orientation. The other parameters are fixed by the usual mechanical characteristics and derived from the material mix.

4. MODELING THE BENDING TEST OF THE CANTILEVER DECK

The mesh used to reproduce experimental results is composed of tetrahedrons elements with linear interpolation functions for a total of 10,355 nodes. The nodes are equally dispatched. The three reinforcing bars are modelled by one equivalent bar, itself modelled by 1D linear perfectly elastic bar elements. The mesh also takes advantage of one symmetric vertical plan. The structural boundary conditions are modelled by means of elastic supports. The displacement of the steel frame is considered by calibrating the stiffness of the elastic supports to match the measured displacement close to the support. Even though the orientation of fibres is not known, we suppose that fibres are mainly aligned ($k_g = 3$, which corresponds to a fibre orientation factor of 70 %) in the deck and uniformly oriented ($k_g \rightarrow 0$,

which corresponds to a fibre orientation factor of 50 %) in the reinforced concrete ribs. The model does not simulate damage in compression; so, along with the hypothesis of perfectly elastic bar elements, it cannot capture the maximal structural strength. The computations are made in the open source Code_Aster finite element code [20].

Figure 5 shows a first comparison, between the test and the simulation, of the force versus the deflection of the deck and two damage states. The first remark is that the experimental test shows an elastic linear behaviour until first cracking at 6 kN and then a second linear behaviour. As for the simulation, the first cracking occurs at 4 kN, and the following non-linear behaviour is slightly curved. The maximal strength measured is 34 kN for the test and 33 kN for the simulation at the same deflection. The hypothesis concerning the steel reinforcement being perfectly elastic is verified since the maximum von Mises stress is 67 MPa < σ_y = 350 MPa.

The damage evolution is shown in Fig. 6 for three different load levels. Damage state (a) refers to initiation of the cracked state. The first crack is located at the left side of second transversal rib. The second crack appears on the right side of the same rib (b). Two following cracks are situated around the third transversal rib. At the advanced damaged state (c), other cracks appear around the second transversal rib, which well corresponds to the observations on the full-scale test.

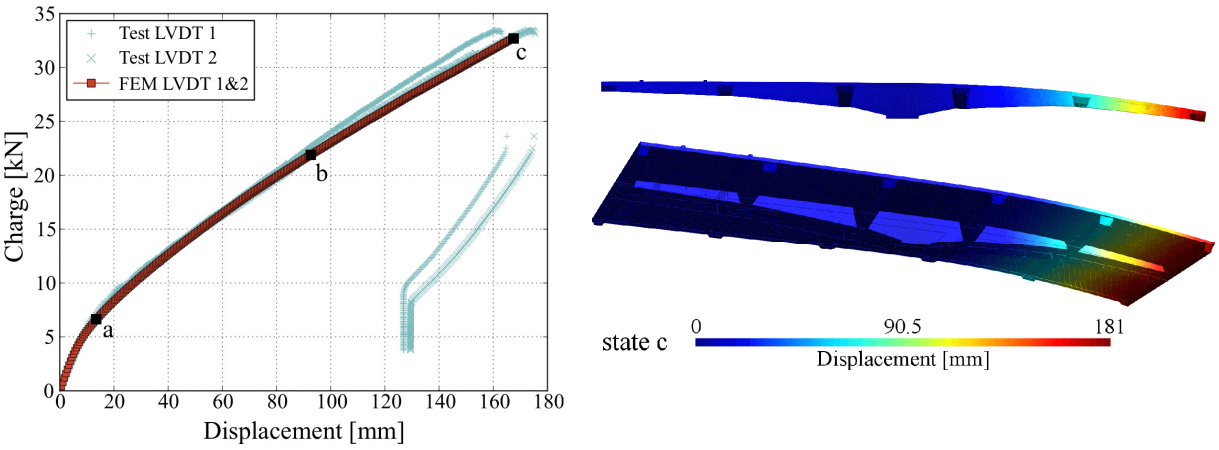

Figure 5: 3D displacement view of the deck at state (c) and experimental test results

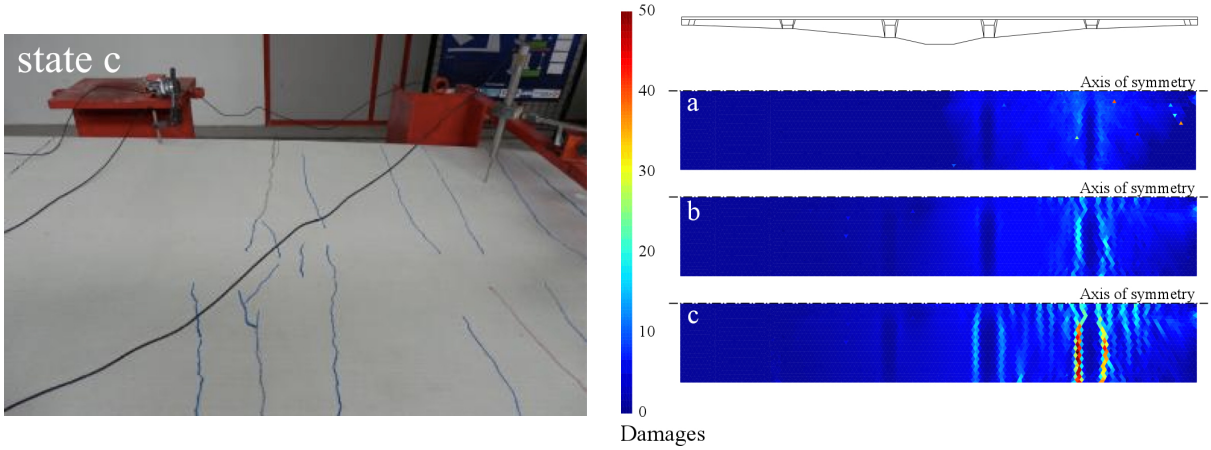

Figure 6: Damage evolution for states (a), (b) and (c) of Fig. 5

Figure 7 shows a comparison between strain gauges dispatched on the structure (Fig. 2) and numerical results. All series of values are captured by the numerical simulation, except for strain gauge No.1. This mismatch can be explained by the fact that this strain is affected by the elastic support, the local coarse mesh and by the absence of damage in compression. In future work, there is a need to model with finer details the boundary condition of the central support by contact elements, in order to better capture the rotation of the central support and to be able to model torsion tests.

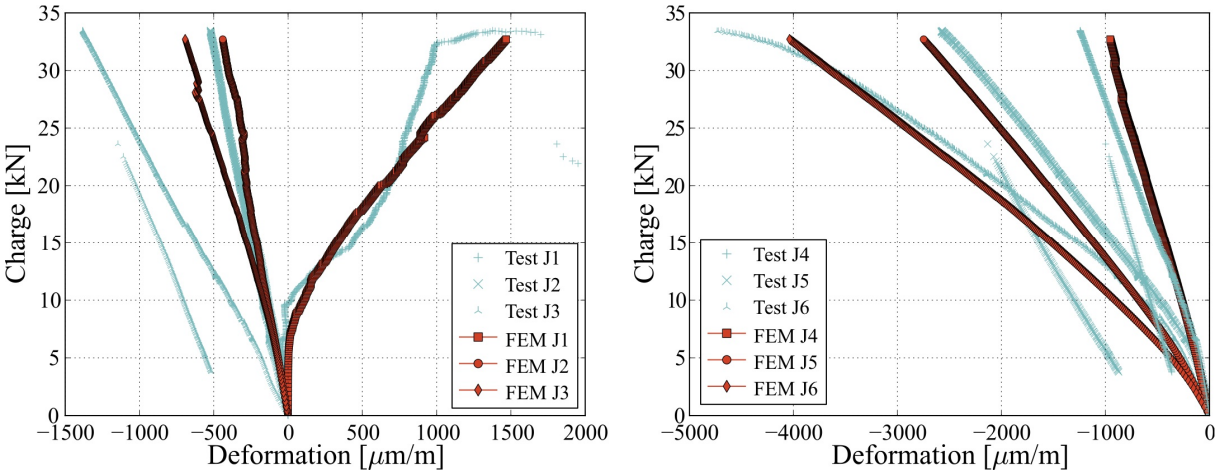

Figure 7: Difference between the experimental results and the numerical simulation of six strain gauges; see Fig. 2 for positions.

Figure 8 shows where the deck broke in compression after a maximal deflection of 178 mm. In the model, there is no damage in compression but the maximal compressive strength of the material (150 MPa) is reached in the exact same location.

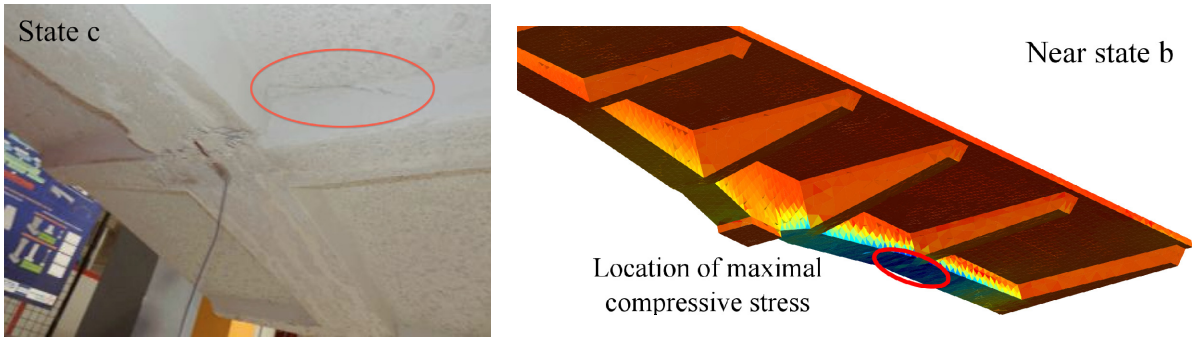

Figure 8: Compression failure of the cantilever deck footbridge

5. EFFECT OF THE CASTING PROCEDURE

To assess the structural sensitivity to the casting procedure, we considered a uniform fibre orientation in the underneath reinforcing ribs, while considering different hypotheses of fibre distribution in the slab. We considered three cases: (i) $k_g \rightarrow 0$ which supposes that fibres are all uniformly oriented which could happen in the case of several filling points being used;

(ii) $k_g = 3$ which is considered as a simple casting, fibres are mainly aligned lengthwise; and (iii) $k_g = 10$ which supposes that fibres were highly longitudinally aligned.

Figure 9 shows the structural response with the three different hypotheses of fibre orientation in the UHPFRC deck with and without steel reinforcement. The fibre orientation of 90% can increase the maximum load of the structure by a maximum factor of 11 % with the steel reinforcement and by a factor of 36 % for the case without steel reinforcement. This suggests the key role of the fibre distribution for the design of such a structure. The casting procedure of such structure should thus be optimized to favour fibre orientation.

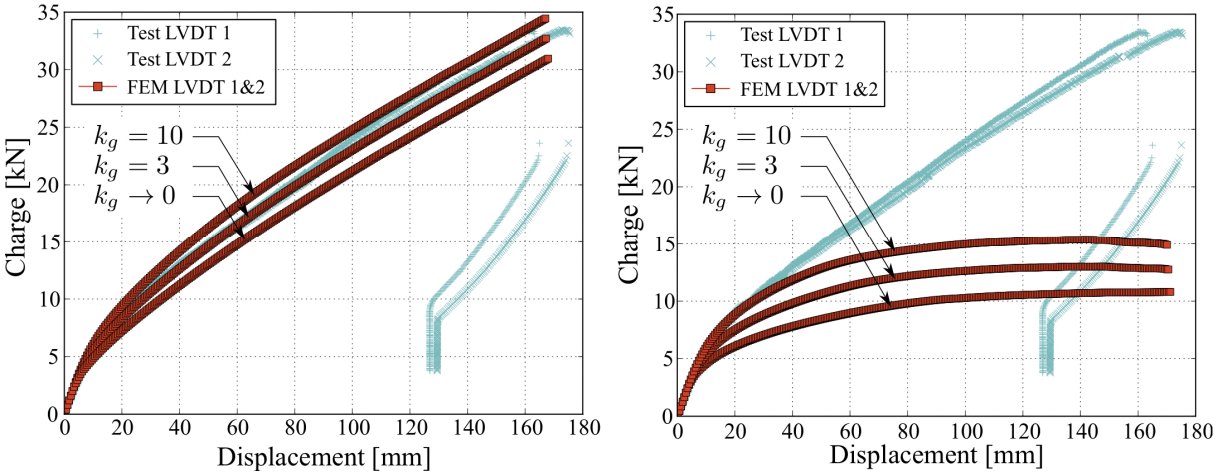

Figure 9: Effect of casting method on the structure response with and without reinforcing bars

6. CONCLUDING REMARKS AND OUTLOOK FOR FUTURE RESEARCH

In this paper, we applied a new fracture-micromechanics model to take into account the effect of fibre orientation in different zones of the structure. The material model also depends on the fibre volume and geometry, matrix fracture energy, fibre-matrix interface characteristics. The fibre orientation is modelled by a probability distribution function of the Gaussian type which makes it possible to reproduce the effect of the casting process. This parameter was related to the more standard fibre orientation factor. The FEM analysis was able to reproduce experimental results, with exception of damage in compressive zones. This preliminary study shows that model-based analysis can be employed to assess the effect of the fibre orientation on real-scale thin UHPFRC structures.

In future works, the torsion behaviour of the structure will be considered. The model will also be improved to account for damage in compression and include a non-local algorithm for assuring mesh objectivity without the need of calibrating a characteristic length towards a more reliable prediction of the effect of fibre orientation on the structural ductility.

ACKNOWLEDGEMENTS

We acknowledge the support of Lafarge Ductal® Paris for having made available the experimental data on the structure. In addition, we acknowledge the CRSNG RDC project framework and UPE-IFSTTAR / Laval University partnership for supporting the current research development.

REFERENCES

[1] Bernier, G. and Behloul, M., 'Effet de l'orientation des fibres sur le comportement des BPR', *Revue française de génie civil*, (1996) 233-240.
[2] Bayard, O., 'Approche multi-échelles du comportement mécanique des bétons à ultra hautes performances renforcés par des fibres courtes', *Ph.D. Thesis, Ecole Normale Supérieure de Cachan, France*, (2003).
[3] Willam, K.J. and Warnke, E.P., 'Constitutive model for the triaxial behaviour of concrete', *Colloquium on Concrete Structures Subjected to Triaxial Stresses, IABSE Report*, **29** (1975) 1-30.
[4] Lubliner, J., Oliver, J., Oller, S. and Oñate, E., 'A plastic-damage model for concrete', *International Journal of Solids and Structures*, **25** (3) (1989) 299-326.
[5] Chen, L., and Graybeal, B.A., 'Finite element analysis of ultra-high performance concrete: Modeling structural performance of an AASHTO type II girder and a 2nd generation pi-girder', *Federal Highway Administration*, (2010).
[6] Feenstra, P.H. and de Borst, R.D., 'A composite plasticity model for concrete', *International Journal of Solids and Structures*, **33** (5) (1996) 707-730.
[7] Li, V.C., Wang, Y., and Backer, S., 'A micromechanical model of tension-softening and bridging toughening of short random fiber reinforced brittle matrix composites', *Journal of the Mechanics and Physics of Solids*, **39** (5) (1991) 607-625.
[8] Lin, Z. and Li, V.C., 'Crack bridging in fiber reinforced cementitious composites with slip-hardening interfaces', *J. Mech. Phys. Solids (UK)*, **45** (5) (1997) 763-787.
[9] Sorelli, L., Ulm, F.J. and Toutlemonde, F., 'Fracture stability and micromechanics of strain hardening cementitious composites', Proceedings of 6th Int. Conf. on Fracture Mechanics of Concrete and Structure (FRAMCOS), (Catania, 2007) 1403-1411.
[10] Sorelli, L., Ulm, F.J. and Guénet, T., 'A new fracture-micromechanics model to account for the effect of fiber distribution on the strain hardening behaviour of fiber reinforced concretes', *Engineering Fracture Mechanics*, (2013) submitted.
[11] Guénet, T., 'Un modèle numérique pour structures en béton fibré à ultra-hautes performances: prise en compte de l'orientation des fibres par une approche d'endommagement micromécanique', *M.Sc. Thesis, Université Laval, Canada*, (2012).
[12] Corvez, D., Ferrier, E., Michel, L., Ammouche, A. and Commene, J.P., 'Ultra-high performance concrete reinforced with stainless steel fibres: from material optimization to structural component response', *Int. Symposium on UHPFRC*, (Marseille, 2013).
[13] Bažant, Z. and Planas, J., 'Fracture and size effect in concrete and other quasibrittle materials', New direction in civil engineering, (CRC Press, 1998).
[14] Budiansky, B. and O'Connell, R.J., 'Elastic moduli of a cracked solid', *International Journal of Solids and Structures*, **12** (2) (1976) 81-97.
[15] Mori, T. and Tanaka, K., 'Average stress in matrix and average elastic energy of materials with misfitting inclusions', *Acta Metallurgica (USA)*, **21** (5) 571-574.
[16] Dormieux, L., Kondo, D. and Ulm, F.J., 'Microporomechanics', (Wiley, 2006).
[17] Naaman, A.E. and Shah, S.P., 'Pull-out mechanism in steel fiber-reinforced concrete', *Journal of the Structural Division*, **102** (8) (1976) 1537-1548.
[18] Leung, C.K.Y. and Li, V.C., 'New strength-based model for the debonding of discontinuous fibres in an elastic matrix', *Journal of Material Science*, **26** (1991) 5996-6010.
[19] Orange, O., Acker, P. and Vernet, C., 'A new generation of UHP concrete: Ductal® damage resistance and micromechanical analysis', *3rd International RILEM Workshop HPFRCC*, (1999)
[20] URL http://www.code-aster.org.